IEEJ Journal of Industry Applications
Vol.7 No.1 pp.35–42 DOI: 10.1541/ieejjia.7.35

Paper

Extremum Co-Energy Principle for Analyzing AC Current Distribution in Parallel-Connected Wires of High-Frequency Power Inductors

Tomohide Shirakawa[*a)] Student Member, Genki Yamasaki[*] Student Member
Kazuhiro Umetani[*] Member, Eiji Hiraki[*] Member

(Manuscript received Jan. 13, 2017, revised Sep. 13, 2017)

Inductor winding is often comprised of parallel-connected wires to suppress copper loss. However, in high-frequency inductors, the proximity effect can cause concentrated AC current distribution, hindering the suppression of the copper loss. Therefore, optimization of the physical inductor structure requires predicting the AC current distribution caused by the proximity effect. Certainly, simulators have been commonly employed for predicting the AC current distribution. However, simple analytical methods are also required for efficient design or invention of inductor structures that have more uniform AC current distribution among the parallel-connected wires. The paper proposes a novel simple analysis method for AC current distribution in parallel-connected wires of high-frequency inductors. The proposed method is based on a novel insight that AC current is distributed to give an extremum of the magnetic co-energy contributed by the AC flux under the given total AC current. Analysis of basic inductor structures revealed that the proposed method can derive the AC current distribution by straightforward calculation. In addition, experiments supported the analysis results. Consequently, the proposed method is suggested to be promising for developing inductor structures with less copper loss.

Keywords: AC current distribution, magnetic co-energy, inductor, magnetic circuit

1. Introduction

The copper loss of power inductors is one of the major power loss in power converters. The copper loss is the Joule loss generated by the DC and AC current. As widely known, the copper loss can be effectively suppressed by designing sufficient wire cross-sectional area of the inductor winding. However, an extremely thick wire may cause difficulty in forming a winding because of its excessive stiffness. Therefore, the winding is often made as parallel-connected wires to increase the wire cross-sectional area [(1)–(7)].

Parallel-connected wires offer effective copper loss reduction particularly for the DC current because the DC current distribution depends on the parasitic resistance. Generally, the DC current in the parallel-connected wires is distributed to achieve the same DC voltage drop among the wires. The DC voltage drop equals to the parasitic resistance multiplied by the DC current. Therefore, the DC current is distributed uniformly among the parallel-connected wires of the same cross-sectional area, leading to effective loss reduction by the DC current.

On the other hand, parallel-connected wires do not necessarily contribute to effective copper loss reduction for the AC current [(1)–(7)]. The AC current is distributed to achieve the same AC voltage drop among the wires. The AC voltage drop equals to the AC impedance multiplied by the AC current. However, the AC impedance generally differs among the parallel-connected wires, even though the wire cross-sectional area is the same. Actually, the AC impedance is rather profoundly affected by the leakage inductance and the complicated magnetic coupling among the wires. As a result, the AC current is not necessarily distributed uniformly among the wires. This mechanism is widely known as the proximity effect.

The proximity effect tends to dominate the AC current distribution particularly in high-frequency operation [(1)(4)(6)–(8)]. In this case, the parallel-connected wires may not effectively reduce the copper loss. This difficulty can be a severe issue particularly in power inductors operated with large AC current at an extremely high frequency.

In spite of this difficulty, recent progress of power electronics has given rise to a number of power converters whose inductors are operated with large AC current at a high frequency. Many of these converters are beneficial in miniaturization of passive components such as inductors and capacitors as well as reduction of switching loss. For example, critical conduction mode boot choppers [(9)–(12)] are widely utilized for the PFC converters. Besides, resonant LLC converters [(13)–(16)] are widely utilized for DC-DC converters operated at a high frequency. However, these converters tend to suffer from large copper loss caused by the large AC current. Therefore, effective suppression of the copper loss is intensely required.

The leakage inductance and the magnetic coupling, which cause the proximity effect, are intensely dependent on the physical structure of the core and the disposition of the

a) Correspondence to: Tomohide Shirakawa. E-mail: prjo4kx3@s.okayama-u.ac.jp
* Okayama University
3-1-1, Tsushimanaka, Kita-ku, Okayama 700-8530, Japan

wires [8][17][18]. Therefore, effective suppression of the copper loss may require design optimization of the inductor structure to achieve a uniform AC current distribution in the parallel-connected wires.

The AC current distribution of magnetic devices has been analyzed and predicted commonly using FEM-based electromagnetic field analysis [4][17][18]. However, numerical calculation may be inconvenient in practical inductor design because of its complicated analysis procedure as well as complicated model construction. Therefore, simple analytical methods may take an important role in practical inductor design.

In contradiction to the FEM analysis, only a few analytical methods have been known to predict the AC current distribution in parallel-connected wires of high-frequency inductors. Certainly, practical analytical methods with simple model construction have been proposed in the preceding works [3][6][7]. However, these methods may still suffer from comparatively complicated calculation process. For example, the method proposed by W. Chen et al. [3] needs numerical calculation of the 1-dimensional magnetic field analysis. The method proposed by R. Prieto et al. [6] partially needs FEM analysis to determine the impedance of each wire.

Certainly, the method proposed by M. Chen et al. [7] is free from magnetic field analysis because this method models planar inductors as lumped circuit models. As a result, this method utilizes the circuit theory for analysis of the AC current distribution. However, analysis by this method may still suffer from complicated calculation because these lumped circuit models tend to have many ideal transformers, each of which represents a wire.

The purpose of this paper is to propose a simple analytical method that allows straightforward calculation based on simple magnetic circuit models. This method can be utilized to predict the AC current distribution in high-frequency inductors, in which the parasitic resistance can be approximated to have an ignorable effect on the AC current distribution.

This proposed method is based on a novel insight proposed in this paper. According to this insight, the AC current is distributed to give an extremum of the magnetic co-energy [19][20] contributed by the AC flux of the inductor under the given total AC current. Hereafter, this insight is referred to as the extremum co-energy principle.

The following discussion consists of 4 sections. Section 2 presents demonstration of the extremum co-energy principle. Section 3 presents the proposed analysis method of the AC current distribution. This section also presents some basic examples of inductors with EI cores. Section 4 presents experiments on these examples to verify the proposed analysis method. Finally, section 5 gives conclusions.

2. Extremum Co-energy Principle

According to the extremum co-energy principle, the AC current in parallel-connected wires is distributed to give an extremum of the magnetic co-energy contributed by the AC flux under the given total AC current. In this principle, the parasitic resistance of the wires is assumed to have an ignorable effect on the AC current distribution. Therefore, the AC current distribution is rather dominantly determined by the leakage inductance and the magnetic coupling of the wires, as is often the cases in high-frequency inductors.

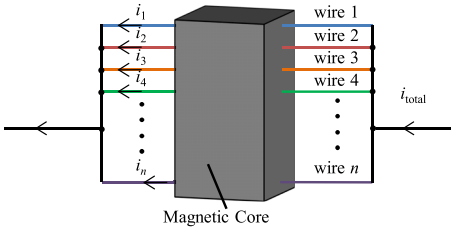

Fig. 1. Generalized inductor model with parallel connected wires

The following discussion considers an inductor with parallel-connected n wires, as shown in Fig. 1. The instantaneous current of wires $1, 2, \ldots, n$ is denoted as $i_1, i_2, \ldots, i_n$, respectively. We introduce the current vector $\mathbf{i}$ defined as $\mathbf{i} = [i_1, i_2, \ldots, i_n]^t$. The flux linkages of these wires are functions of $\mathbf{i}$. Therefore, we denote them as $\psi_1(\mathbf{i})$, $\psi_2(\mathbf{i})$, $\ldots$, $\psi_n(\mathbf{i})$, respectively. In addition, we introduce the flux linkage vector $\boldsymbol{\psi}$ defined as $\boldsymbol{\psi} = [\psi_1, \psi_2, \ldots, \psi_n]^t$.

Then, the total magnetic co-energy E of this inductor can be expressed as

$$E(\mathbf{i}) = \int_{\mathbf{0}}^{\mathbf{i}} \boldsymbol{\psi} \cdot d\mathbf{i}. \quad \cdots\cdots (1)$$

We regard current i_1, i_2, $\ldots$, i_n as the sum of the DC current $I_1, I_2, \ldots, I_n$ and the instantenous AC current $i_{\text{ac}1}, i_{\text{ac}2}, \ldots, i_{\text{ac}n}$, respectively. We further regard the flux linkage $\psi_1, \psi_2, \ldots, \psi_n$ as the sum of the DC flux linkage $\psi_{\text{dc}1}, \psi_{\text{dc}2}, \ldots, \psi_{\text{dc}n}$ and the AC flux linkage $\psi_{\text{ac}1}, \psi_{\text{ac}2}, \ldots, \psi_{\text{ac}n}$, respectively. The DC current $I_1, I_2, \ldots, I_n$ are assumed to be given. The DC flux linkage $\psi_{\text{dc}1}, \psi_{\text{dc}2}, \ldots, \psi_{\text{dc}n}$ are also assumed to be given, because the DC flux linkage can be determined by the given DC current distribution.

We define the DC current vector $\mathbf{I}$ and the AC current vector $\mathbf{i}_{\text{ac}}$ as $\mathbf{I} = [I_1, I_2, \ldots, I_n]^t$ and $\mathbf{i}_{\text{ac}} = [i_{\text{ac}1}, i_{\text{ac}2}, \ldots, i_{\text{ac}n}]^t$, respectively. Hence, $\mathbf{i} = \mathbf{I} + \mathbf{i}_{\text{ac}}$. We also define the DC flux linkage vector $\boldsymbol{\psi}_{\text{dc}}$ and the AC flux linkage vector $\boldsymbol{\psi}_{\text{ac}}$ as $\boldsymbol{\psi}_{\text{dc}} = [\psi_{\text{dc}1}, \psi_{\text{dc}2}, \ldots, \psi_{\text{dc}n}]^t$ and $\boldsymbol{\psi}_{\text{ac}} = [\psi_{\text{ac}1}, \psi_{\text{ac}2}, \ldots, \psi_{\text{ac}n}]^t$, respectively. Hence, $\boldsymbol{\psi} = \boldsymbol{\psi}_{\text{dc}} + \boldsymbol{\psi}_{\text{ac}}$.

Then, (1) can be rewritten as

$$\begin{aligned} E(\mathbf{I}, \mathbf{i}_{\text{ac}}) &= \int_{\mathbf{0}}^{\mathbf{I}} \boldsymbol{\psi} \cdot d\mathbf{i} + \int_{\mathbf{I}}^{\mathbf{I}+\mathbf{i}_{\text{ac}}} \boldsymbol{\psi} \cdot d\mathbf{i} \\ &= E_{\text{dc}}(\mathbf{I}) + \boldsymbol{\psi}_{\text{dc}} \cdot \mathbf{i}_{\text{ac}} + E_{\text{ac}}(\mathbf{I}, \mathbf{i}_{\text{ac}}), \quad \cdots\cdots (2) \end{aligned}$$

where E_{dc} is a function of $\mathbf{I}$ and E_{ac} is a function of $\mathbf{I}$ and $\mathbf{i}_{\text{ac}}$ defined as

$$E_{\text{dc}}(\mathbf{I}) = \int_{\mathbf{0}}^{\mathbf{I}} \boldsymbol{\psi} \cdot d\mathbf{i}, \quad \cdots\cdots (3)$$

$$E_{\text{ac}}(\mathbf{I}, \mathbf{i}_{\text{ac}}) = \int_{\mathbf{I}}^{\mathbf{I}+\mathbf{i}_{\text{ac}}} \boldsymbol{\psi}_{\text{ac}} \cdot d\mathbf{i} = \int_{\mathbf{0}}^{\mathbf{i}_{\text{ac}}} \boldsymbol{\psi}_{\text{ac}}(\mathbf{I}, \mathbf{i}_{\text{ac}}) \cdot d\mathbf{i}_{\text{ac}}. \quad \cdots\cdots (4)$$

The requirement of the given total AC inductor current can be expressed using $i_{\text{ac}1}, i_{\text{ac}2}, \ldots, i_{\text{ac}n}$ as

$$i_{\text{ac\_total}} = \sum_{k=1}^{n} i_{\text{ac}\,k}, \quad \cdots\cdots (5)$$

where k is the index of the wires, and $i_{\text{ac\_total}}$ is the given total AC current. $E_{\text{ac}}(\mathbf{I}, \mathbf{i}_{\text{ac}})$ is the magnetic co-energy contributed by the AC flux. Therefore, the extremum co-energy principle

requires $E_{ac}(\mathbf{I}, \mathbf{i}_{ac})$ to take an extremum under the given total AC current i_{ac_total}.

Now, we seek for the solution of $\mathbf{i}_{ac}$ that gives an extremum of $E(\mathbf{I}, \mathbf{i}_{ac})$ under given i_{ac_total}. This solution can be obtained using the Lagrangian multiplier method. We introduce $E'(\mathbf{I}, \mathbf{i}_{ac}, \lambda)$ defined as

$$E'(\mathbf{I}, \mathbf{i}_{ac}, \lambda) = E_{ac}(\mathbf{I}, \mathbf{i}_{ac}) + \lambda\left(i_{ac\_total} - \sum_{k=1}^{n} i_{ack}\right), \quad \cdots\cdots (6)$$

where λ is the Lagrangian multiplier. Then, the solution of $\mathbf{i}_{ac}$ must give an extremum of E'. Therefore, the solution meets the following requirement:

$$\frac{\partial E'}{\partial i_{ac1}} = \frac{\partial E'}{\partial i_{ac2}} = \cdots = \frac{\partial E'}{\partial i_{acn}} = \frac{\partial E'}{\partial \lambda} = 0. \cdots\cdots (7)$$

As a result, we obtain (5) and the following relation:

$$\psi_{ac1} = \psi_{ac2} = \cdots = \psi_{acn} = \lambda. \cdots\cdots (8)$$

Equation (8) indicates that the AC flux linkage in all the wires must be the same. This requirement is consistent with Kirchhoff's voltage law applied to the parallel-connected wires, because the time derivative of the AC flux linkage of a wire equals to the voltage induced in the wire, according to Faraday's law.

On the other hand, (5) corresponds to Kirchhoff's current law. Noting that $\psi_{ac1}, \psi_{ac2}, \ldots, \psi_{acn}$ are the functions of $i_{ac1}, i_{ac2}, \ldots, i_{acn}$, we can obtain the solution of $i_{ac1}, i_{ac2}, \ldots, i_{acn}$ from (5) and (8). In fact, (5) and (8) suffice to determine all of $i_{ac1}, i_{ac2}, \ldots, i_{acn}$ because (5) and (8) give $n + 1$ equations of $n + 1$ unknown parameters, i.e. $i_{ac1}, i_{ac2}, \ldots, i_{acn}, \lambda$.

Consequently, the extremum co-energy principle is shown to be consistent with Kirchhoff's voltage law. This indicates the appropriateness of this principle. Furthermore, the extremum co-energy principle in combination with Kirchhoff's current law suffices to determine the AC current distribution in the parallel-connected wires.

3. Proposed Analysis Method of AC Current Distribution

3.1 Proposed Method According to the extremum co-energy principle, we can determine the AC current distribution based on the magnetic circuit model. In the magnetic circuit model, the magnetomotive force follows Kirchhoff's voltage law; and the flux follows the Kirchhoff's current law. Therefore, we can easily solve the flux passing through the reluctance using the circuit theory. As a result, we obtain the AC flux as functions of the AC current of the wires.

Then, the total magnetic co-energy contributed by the AC flux can be obtained from this solution of the AC flux. For convenience, we neglect the magnetic saturation. Hence, the reluctance is assumed to be constant. Under this assumption, the AC flux linkage $\psi_{ac1}, \psi_{ac2}, \ldots, \psi_{acn}$ is independent on the DC current $\mathbf{I}$. Therefore, the magnetic co-energy contributed by the AC flux equals to the total magnetic co-energy under the condition in which only AC current and no DC current flows in the winding.

The total magnetic co-energy is the sum of the co-energy contributed by all the reluctance. As for the reluctance $\mathcal{R}$, through which only AC flux ϕ_{ac} passes, the magnetic co-energy contributed by this reluctance can be expressed as $\mathcal{R}{\phi_{ac}}^2/2$. Because the AC flux is a function of the AC current, the total magnetic co-energy at no DC current is a function of the AC current of the wires.

According to the extremum co-energy principle, the solution of the AC current distribution must give an extremum of the magnetic co-energy at no DC current without changing the total AC current. This solution can be obtained as follows. Let $E(i_{ac1}, i_{ac2}, \ldots, i_{acn})$ be the total magnetic co-energy at no DC current given as a function of the instantaneous AC wire current $i_{ac1}, i_{ac2}, \ldots, i_{acn}$; and let i_{ac_total} be the given total instantaneous AC current.

According to the Lagrangian multiplier method, we introduce modified magnetic co-energy $E'(i_{ac1}, i_{ac2}, \ldots, i_{acn}, \lambda)$ defined as

$$E'(i_{ac1}, i_{ac2}, \cdots, i_{acn}, \lambda) = E(i_{ac1}, i_{ac2}, \cdots, i_{acn}, \lambda) + \lambda(i_{ac1} + i_{ac2} + \cdots + i_{acn} - i_{ac\_total}). \cdots\cdots (9)$$

Then, the solution can be obtained by solving the following relation:

$$\frac{\partial E'}{\partial i_{ac1}} = \frac{\partial E'}{\partial i_{ac2}} = \cdots = \frac{\partial E'}{\partial i_{acn}} = \frac{\partial E'}{\partial \lambda} = 0. \cdots\cdots (10)$$

The result gives $n + 1$ equations of $n + 1$ unknown parameters, i.e. $i_{ac2}, \ldots, i_{acn}, \lambda$. Therefore, we can determine the AC current of all the wires.

3.2 Example 1 We consider an inductor with two parallel-connected wires wound on a pair of EI cores as shown in Fig. 2. The cores have gaps on the center and outer legs. The winding consists of two winding layers, each of which is formed of a wire and has the same number of turns N. We denote the wire that forms the winding layer closer to the gaps as wire 1; and we denote the other as wire 2.

The magnetic circuit model of Fig. 2 is constructed by applying Dowell's approximation [21]–[29]. This approximation is effective to simplify the model construction of the planar magnetic devices with uniformly wound winding layers. In addition, appropriateness of the resultant models have been verified in many preceding studies [21]–[29].

According to this approximation, we assume 2 dimensional magnetic field based on the vertical cross-section view of the magnetic core. In addition, we assume that all the magnetic flux paths can be classified into only two categories: One is the flux path passing through the magnetic core, and the other is the flux path passing between the winding layers or between the winding layer and the magnetic core. Furthermore, uniform magnetic flux distribution is assumed along

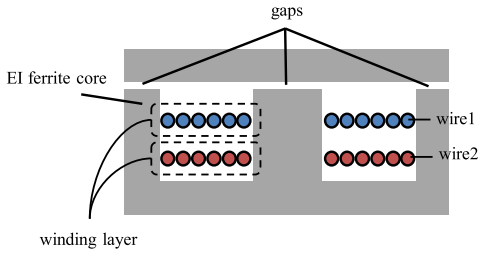

Fig. 2. Cross-section view of the inductor of example 1

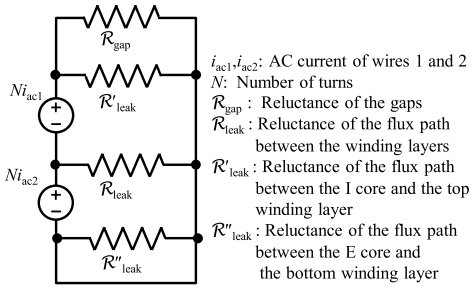

Fig. 3. Magnetic circuit model of the inductor of example 1

the winding layers.

The vertical cross-section of the EI core has the mirror symmetry with respect to the center line. Hence, the left half of Fig. 2 has the same magnetic flux distribution and the same magnetic co-energy as those of the right half. Therefore, we only need to construct the magnetic circuit model of the left half of Fig. 2 because the condition of the extremum co-energy for the left half is the same as that for the whole magnetic structure.

For convenience, we assume that the magnetic cores have far greater permeability compared with the gaps and the leakage flux path; and therefore, we ignore the reluctance contributed by the magnetic cores. In addition, we assume that all the height of the area between the neighboring winding layers are the same so that the flux paths passing through these area have the same reluctance. As a result, we obtain the magnetic circuit model of this inductor as shown in Fig. 3. Reluctance $\mathcal{R}_{gap}$ is the reluctance of the flux path passing through the gaps, whereas $\mathcal{R}_{leak}$ is the reluctance of the flux path passing through the area between the winding layers. Reluctance $\mathcal{R}'_{leak}$ and $\mathcal{R}''_{leak}$ are the reluctance of the flux path passing through the area between the I core and the top winding layer and that between the E core and the bottom winding layer, respectively. Current i_{ac1} and i_{ac2} are the instantaneous AC current of wire 1 and 2, respectively.

Note that no flux passes through $\mathcal{R}''_{leak}$. Therefore, the total magnetic co-energy E_{ex1} for Fig. 3 at no DC current can be expressed as

$$E_{ex1} = \frac{(Ni_{ac1} + Ni_{ac2})^2}{2\mathcal{R}'_{gap}} + \frac{N^2 i_{ac2}^2}{2\mathcal{R}_{leak}}, \cdots\cdots\cdots\cdots (11)$$

where $\mathcal{R}'_{gap}$ is the equivalent impedance of the parallel connection of $\mathcal{R}_{gap}$ and $\mathcal{R}'_{leak}$. Hence, $\mathcal{R}'_{gap} = \mathcal{R}_{gap}\mathcal{R}'_{leak}/(\mathcal{R}_{gap} + \mathcal{R}'_{leak})$.

We seek for the solution of i_{ac1} and i_{ac2} that gives an extremum of E_{ex1} under the given total instantaneous AC current i_{ac_total}. Then, the modified magnetic co-energy E'_{ex1} is obtained as

$$E'_{ex1} = \frac{(Ni_{ac1}+Ni_{ac2})^2}{2\mathcal{R}'_{gap}} + \frac{N^2 i_{ac2}^2}{2\mathcal{R}_{leak}} + \lambda\,(i_{ac1}+i_{ac2}-i_{ac\_total})\,. \cdots\cdots\cdots\cdots (12)$$

Applying (12) to (10) yields following equations:

$$\frac{N^2\,(i_{ac1} + i_{ac2})}{\mathcal{R}'_{gap}} = -\lambda, \quad \frac{N^2\,(i_{ac1} + i_{ac2})}{\mathcal{R}'_{gap}} + \frac{N^2 i_{ac2}}{\mathcal{R}_{leak}} = -\lambda,$$
$$i_{ac1} + i_{ac2} = i_{ac\_total}. \cdots\cdots\cdots\cdots (13)$$

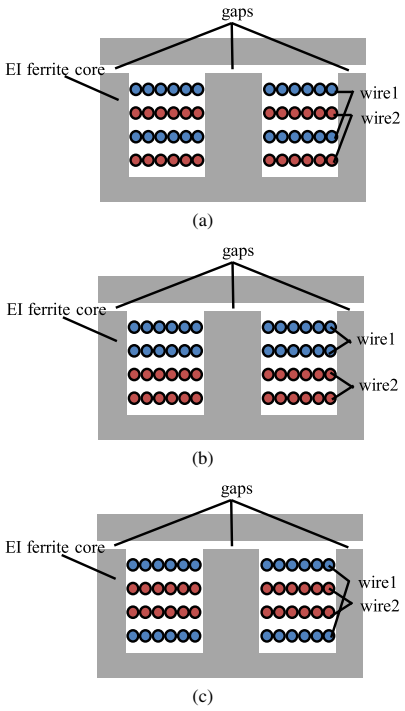

Fig. 4. Cross-section views of the inductor of example 2

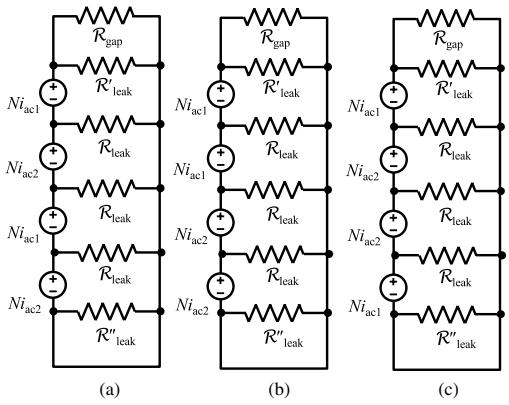

i_{ac1}, i_{ac2}: AC current of wires 1 and 2
N: Number of turns per layer
$\mathcal{R}_{gap}$: Reluctance of the gaps
$\mathcal{R}_{leak}$: Reluctance of the flux path between neighboring winding layers
$\mathcal{R}'_{leak}$: Reluctance of the flux path between the I core and the top winding layer
$\mathcal{R}''_{leak}$: Reluctance of the flux path between the E core and the bottom winding layer

Fig. 5. Magnetic circuit models of the inductors of example 2

Solving (13), we obtain $i_{ac1} = i_{ac\_total}$ and $i_{ac2} = 0$. Therefore, all the current will flow in wire 1, which is the wire close to the gaps.

3.3 Example 2 Next, we analyze three other inductors, each of which has two parallel-connected wires wound on a pair of EI cores as shown in Fig. 4. The winding consists of four winding layers. Each wire forms two series-connected winding layers. In these examples, each winding layer has the same number of turns. However, the order of the winding layers differs among Fig. 4(a), Fig. 4(b), and Fig. 4(c).

The magnetic circuit models of Fig. 4 are presented in Fig. 5. First, we analyze Fig. 5(a). The total magnetic

co-energy E_{ex2a} for Fig. 5(a) at no DC current is

$$E_{ex2a} = \frac{(2Ni_{ac1} + 2Ni_{ac2})^2}{2\mathcal{R}'_{gap}} + \frac{(Ni_{ac1} + 2Ni_{ac2})^2}{2\mathcal{R}_{leak}} + \frac{(Ni_{ac1} + Ni_{ac2})^2}{2\mathcal{R}_{leak}} + \frac{N^2 i_{ac2}^2}{2\mathcal{R}_{leak}}. \quad \cdots\cdots (14)$$

We seek for the solution of i_{ac1} and i_{ac2} that gives an extremum of E_{ex2a} without changing the total instantaneous inductor current i_{ac_total}. The modified magnetic co-energy E'_{ex2a} is obtained as

$$E'_{ex2a} = \frac{(2Ni_{ac1} + 2Ni_{ac2})^2}{2\mathcal{R}'_{gap}} + \frac{(Ni_{ac1} + 2Ni_{ac2})^2}{2\mathcal{R}_{leak}} + \frac{(Ni_{ac1}+Ni_{ac2})^2}{2\mathcal{R}_{leak}} + \frac{N^2 i_{ac2}^2}{2\mathcal{R}_{leak}} + \lambda\,(i_{ac1}+i_{ac2}-i_{ac\_total})\,. \quad \cdots\cdots (15)$$

Applying (15) to (10) yields

$$\frac{4N^2\,(i_{ac1} + i_{ac2})}{\mathcal{R}'_{gap}} + \frac{N^2\,(2i_{ac1} + 3i_{ac2})}{\mathcal{R}_{leak}} = -\lambda,$$
$$\frac{4N^2\,(i_{ac1} + i_{ac2})}{\mathcal{R}'_{gap}} + \frac{N^2\,(3i_{ac1} + 6i_{ac2})}{\mathcal{R}_{leak}} = -\lambda,$$
$$i_{ac1} + i_{ac2} = i_{ac\_total}. \quad \cdots\cdots (16)$$

The solution of (16) can be obtained as

$$i_{ac1} = \frac{3}{2} i_{ac\_total}, \quad i_{ac2} = -\frac{1}{2} i_{ac\_total}. \quad \cdots\cdots (17)$$

This result indicates that the opposite current flows (or the phase of the current is delayed by π) in wire 2. Therefore, this disposition of the wires even increases the AC copper loss compared with the inductor with only one wire.

Next, we analyze Fig. 5(b). The total magnetic co-energy E_{ex2b} for Fig. 5(b) at no DC current is

$$E_{ex2b} = \frac{(2Ni_{ac1} + 2Ni_{ac2})^2}{2\mathcal{R}'_{gap}} + \frac{(Ni_{ac1} + 2Ni_{ac2})^2}{2\mathcal{R}_{leak}} + \frac{4N^2 i_{ac2}^2}{2\mathcal{R}_{leak}} + \frac{N^2 i_{ac2}^2}{2\mathcal{R}_{leak}}. \quad \cdots\cdots (18)$$

Then, the modified co-energy E'_{ex2c} is obtained as

$$E'_{ex2b} = \frac{(2Ni_{ac1} + 2Ni_{ac2})^2}{2\mathcal{R}'_{gap}} + \frac{(Ni_{ac1} + 2Ni_{ac2})^2}{2\mathcal{R}_{leak}} + \frac{4N^2 i_{ac2}^2}{2\mathcal{R}_{leak}} + \frac{N^2 i_{ac2}^2}{2\mathcal{R}_{leak}} + \lambda\,(i_{ac1} + i_{ac2} - i_{ac\_total})\,. \quad \cdots\cdots (19)$$

Applying (19) into (10) yields

$$\frac{4N^2\,(i_{ac1} + i_{ac2})}{\mathcal{R}'_{gap}} + \frac{N^2\,(i_{ac1} + 2i_{ac2})}{\mathcal{R}_{leak}} = -\lambda,$$
$$\frac{4N^2\,(i_{ac1} + i_{ac2})}{\mathcal{R}'_{gap}} + \frac{N^2\,(2i_{ac1} + 9i_{ac2})}{\mathcal{R}_{leak}} = -\lambda,$$
$$i_{ac1} + i_{ac2} = i_{ac\_total}. \quad \cdots\cdots (20)$$

The solution of (20) can be obtained as

$$i_{ac1} = \frac{7}{6} i_{ac\_total}, \quad i_{ac2} = -\frac{1}{6} i_{ac\_total}. \quad \cdots\cdots (21)$$

Finally, we analyze Fig. 5(c). The total magnetic co-energy E_{ex2c} for Fig. 5(c) at no DC current is

$$E_{ex2c} = \frac{(2Ni_{ac1} + 2Ni_{ac2})^2}{2\mathcal{R}'_{gap}} + \frac{(Ni_{ac1} + 2Ni_{ac2})^2}{2\mathcal{R}_{leak}} + \frac{(Ni_{ac1} + Ni_{ac2})^2}{2\mathcal{R}_{leak}} + \frac{N^2 i_{ac1}^2}{2\mathcal{R}_{leak}}. \quad \cdots\cdots (22)$$

Then, the modified magnetic co-energy E'_{ex2b} is obtained as

$$E'_{ex2c} = \frac{(2Ni_{ac1} + 2Ni_{ac2})^2}{2\mathcal{R}'_{gap}} + \frac{(Ni_{ac1} + 2Ni_{ac2})^2}{2\mathcal{R}_{leak}} + \frac{(Ni_{ac1}+Ni_{ac2})^2}{2\mathcal{R}_{leak}} + \frac{N^2 i_{ac1}^2}{2\mathcal{R}_{leak}} + \lambda\,(i_{ac1}+i_{ac2}-i_{ac\_total})\,. \quad \cdots\cdots (23)$$

Applying (23) into (10) yields

$$\frac{4N^2\,(i_{ac1} + i_{ac2})}{\mathcal{R}'_{gap}} + \frac{N^2\,(3i_{ac1} + 3i_{ac2})}{\mathcal{R}_{leak}} = -\lambda,$$
$$\frac{4N^2\,(i_{ac1} + i_{ac2})}{\mathcal{R}'_{gap}} + \frac{N^2\,(3i_{ac1} + 5i_{ac2})}{\mathcal{R}_{leak}} = -\lambda,$$
$$i_{ac1} + i_{ac2} = i_{ac\_total}. \quad \cdots\cdots (24)$$

The solution of (24) can be obtained as

$$i_{ac1} = i_{ac\_total}, \quad i_{ac2} = 0. \quad \cdots\cdots (25)$$

The results obtained as (17), (21), and (25) indicate that the opposite current in wire 2 is greatly reduced in Fig. 4(b) and Fig. 4(c) compared with Fig. 4(a). Therefore, Fig. 4(b) and Fig. 4(c) are preferable to Fig. 4(a), although both of the inductor structures suffer from concentration of the AC current. If we compare Fig. 4(b) and Fig. 4(c), Fig. 4(c) is preferable because no opposite current flows in wire 2. However, the difference between Fig. 4(b) and Fig. 4(c) is more subtle than that between Fig. 4(a) and Fig. 4(c) because Fig. 4(b) has far smaller opposite current in wire 2 than Fig. 4(a).

4. Experiment

Experiments were carried out to verify the proposed method. In the experiments, examples 1 and 2 presented in the previous section were tested.

4.1 Example 1 First, we tested example 1. Figure 6 shows the experimental inductor constructed on a pair of EI cores. Specifications of the inductor are shown in Table 1. The winding was comprised of two parallel-connected wires of Litz wire ($\phi 0.1 \times 57$ strands). Each wire forms a winding layer of 7 turns. The length of the gaps was set at 1 mm. The height of the space between the winding layers was set at 1 mm.

We applied the AC voltage with the frequency of 100 kHz to the experimental inductors. The total AC inductor current was set at 0.50 Arms. Then, the AC wire current was measured using Rogowski coils.

Figure 7 shows the experimental result of the AC current i_{ac1} and i_{ac2}. In this figure, i_{ac1} and i_{ac2} are expressed as phasors plotted on the complex plane. The phase zero is defined as the phase of the total AC current i_{ac_total}; and the absolute value of the phasors equals to the effective value of the AC current. As can be seen in the figure, both i_{ac1} and i_{ac2}

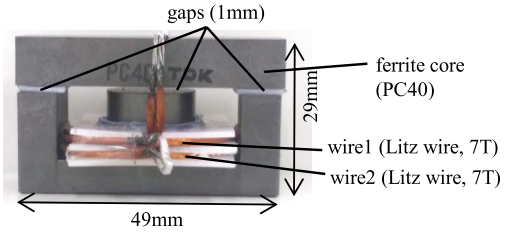

Fig. 6. Photograph of the experimental inductor of example 1

Table 1. Specifications of the inductor of example 1

Inductance	14.7μH
Litz wire (wire 1 and wire 2)	Sumitomo Electric Lz 1-FEIW-N ϕ0.1×57
Number of turns per layer	7T
Outer diameter of winding layers	35mm
Inner diameter of winding layers	20mm
Height of the space between the winding layers	1mm
Material of the bobbin for the winding	polyethylene
Size of the E core	19×49×17mm
Size of the I core	9×49.5×14mm
Magnetic material	TDK PC40
Length of the gaps	1mm
Gap material	polyethylene

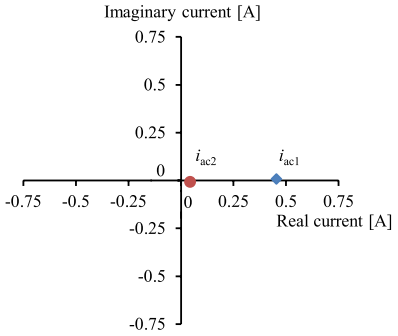

Fig. 7. Experimental result of the AC current in the inductor of example 1. The AC current was plotted as phasors on the complex plane

are plotted close to the real axis. Furthermore, the absolute value for i_{ac1} is far greater than i_{ac2}, indicating that almost all the AC current flows in wire 1. Therefore, the experimental result was consistent with the theory, supporting appropriateness of the proposed method.

4.2 Example 2 Next, we tested example 2. Figure 8 shows three experimental inductors constructed on a pair of EI cores. Specifications of these inductors are shown in Table 2. These inductors have the winding of two parallel-connected wires of Litz wire ($\phi 0.1 \times 57$ strands), similarly as in example 1. Each wire forms two series-connected winding layers of 6 turns. The length of the gaps was set at 1 mm. The height of the spaces between the winding layers was set at 0.5 mm.

We evaluated the AC current distribution in the parallel-connected wires. We again applied the AC voltage with the frequency of 100 kHz to the inductors. The total AC current was set at 1.0 Arms.

Figure 9 shows the experimental result of the AC current

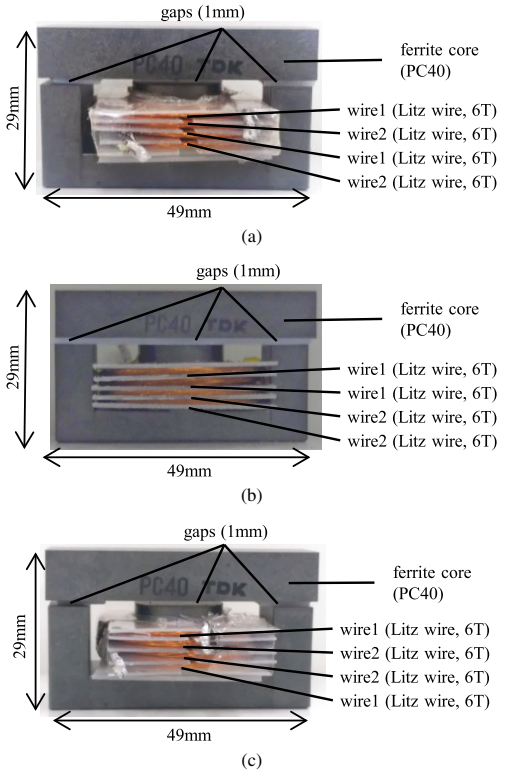

Fig. 8. Photographs of the experimental inductors of example 2

Table 2. Table 2 Specifications of the inductors of example 2

Inductance of Fig. 8(a)	34.4μH
Inductance of Fig. 8(b)	34.7μH
Inductance of Fig. 8(c)	35.2μH
Litz wire (wire 1 and wire 2)	Sumitomo Electric Lz 1-FEIW-N ϕ0.1×57
Number of turns per layer	6T
Outer diameter of winding layers	33 mm
Inner diameter of winding layers	20 mm
Heigth of the space between the winding layers	0.5 mm
Material of the bobbin for the winding	polyethylene
Size of the E core	19×49×17 mm
Size of the I core	9×49.5×14 mm
Magnetic material	TDK PC40
Length of the gaps	1 mm
Gap material	polyethylene

i_{ac1} and i_{ac2}. Similarly as in the previous subsection, i_{ac1} and i_{ac2} are expressed as phasors plotted on the complex plane, in which the phase zero is defined as the phase of the total AC current i_{ac_total}. Similarly as in example 1, both i_{ac1} and i_{ac2} are plotted close to the real axis, which is consistent with the theory.

Next, the AC current distribution was compared between the experimental result and the theoretical prediction. For this purpose, we neglected the imaginary part of the experimental phasors of i_{ac1} and i_{ac2}; and we calculated the ratio of the real part of i_{ac2} to that of the total AC current. Then, this ratio was compared with the theory discussed in subsection 3.3.

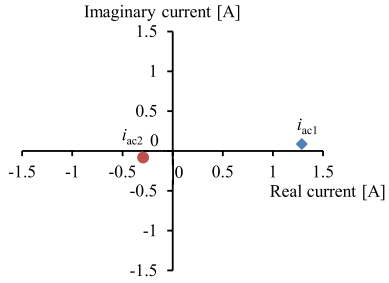

(a) AC Current of Fig. 8(a)

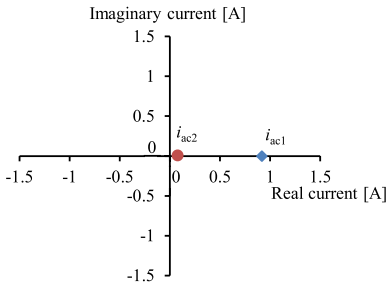

(b) AC current of Fig. 8(b)

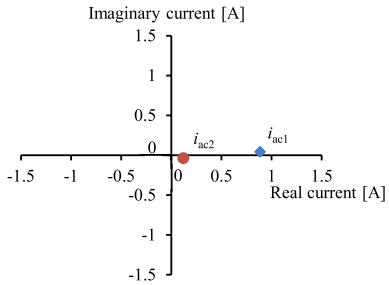

(c) AC Current of Fig. 8(c)

Fig. 9. Experimental results of the AC current in the inductors of example 2. The AC current was plotted as phasors on the complex plane

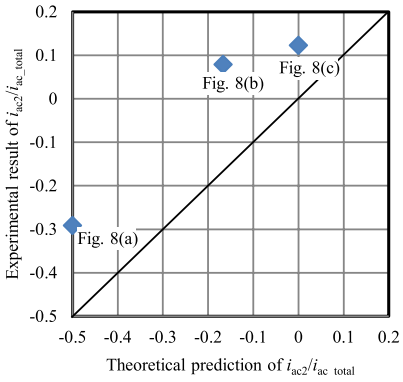

Fig. 10. Experimental result and theoretical prediction of the ratio of the real part of the phasor of the AC current in wire 2 (i_{ac2}) to that of the total AC current (i_{ac_total})

Figure 10 shows the result. Although the experimental result of the ratio was slightly larger than that of the theoretical prediction, dependency of the ratio on the winding disposition was consistent between the experiment and the theory. This slight deviation from the theory may be caused by leakage flux paths not incorporated in the magnetic circuit models because the theoretical prediction was made based on extremely simple magnetic circuit models to simplify the theoretical analysis.

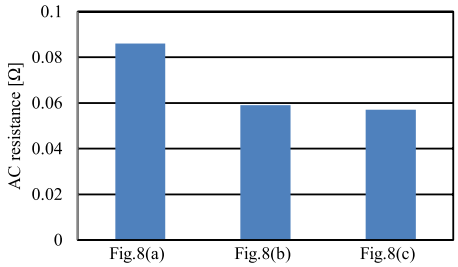

Fig. 11. Experimental result of the AC resistance of the inductors of example 2

In addition, we measured the AC resistance of the experimental inductors at 100 kHz with an LCR-meter. Certainly, the AC resistance is contributed not only by the copper loss but also by the iron loss. However, difference in the copper loss will be reflected in the AC resistance because the iron loss is hardly dependent on the winding disposition and therefore the iron loss will be almost the same among the experimental inductors.

The measurement result of the AC resistance is shown in Fig. 11. The result revealed that Fig. 8(c) showed the least AC resistance. The difference between Fig. 8(b) and Fig. 8(c) was subtle compared with the difference between Fig. 8(a) and Fig. 8(c). These features were also consistent with the theory.

Consequently, these experimental results supported appropriateness of the proposed method and suggested that the proposed method can be utilized to choose the winding disposition with least AC resistance.

5. Conclusions

Parallel-connected wires are commonly utilized for the inductor winding to suppress the copper loss. However, the proximity effect can cause concentration of AC current in one wire, hindering effective suppression of the AC copper loss. Therefore, predicting the AC current distribution is required to optimize the inductor structure. In order to provide a straightforward method to predict the AC current distribution, this paper proposed a novel analysis method based on the extremum co-energy principle. The experiment supported appropriateness of the proposed method. Furthermore, the experiment suggested that the proposed method can be utilized to choose the winding disposition with least AC resistance. Consequently, the proposed method is promising for analyzing the AC current distribution in parallel-connected wires to optimize the inductor structure.

Acknowledgment

This work was supported by Electric Technology Research Foundation of Chugoku.

References

(1) R. Prieto, J.A. Cobos, O. Garcia, P. Alou, and J. Uceda: “Using parallel windings in planar magnetic components”, Proc. IEEE Power Electron. Specialist Conf. (PESC), Vol.04, pp.2055–2060 (2001)

(2) Y. Hu, J. Guan, X. Bai, and W. Chen: “Problems of paralleling windings for planar transformers and solutions”, Proc. IEEE Power Electron. Specialist Conf. (PESC), Vol.2, pp.597–601 (2002)

(3) W. Chen, Y. Yan, Y. Hu, and Q. Lu: “Model and design of pcb parallel winding for planar transformer”, *IEEE Trans. Magn.*, Vol.39, No.05, pp.3202–3204 (2003)

(4) D. Fu, F.C. Lee, and S. Wang: "Investigation on transformer design of high frequency high efficiency DC-DC converters", Proc. Appl. Power Electron. Conf. Expo. (APEC), pp.940–947 (2010)

(5) X. Margueron, A. Besri, Y. Lembeye, and J.P. Keradec: "Current sharing between parallel turns of a planar transformer: prediction and improvement using a circuit simulation software", *IEEE Trans. Ind. Appl*., Vol.46, No.3, pp.1064–1071 (2010)

(6) R. Prieto, R. Asensi, and J.A. Cobos: "Selection of the appropriate winding setup in planar inductors with parallel windings", Proc. IEEE Energy Conversion Congr. Expo. (ECCE), pp.4599–4604 (2010)

(7) M. Chen, M. Araghchini, K.K. Afridi, J.H. Lang, C.R. Sullivan, and D.J. Perreault: "A systematic approach to modeling impedances and current distribution in planar magnetics", *IEEE Trans. Power Electron*., Vol.31, No.1, pp.560–580 (2016)

(8) J.D. van Wyk, Jr., W.A. Cronje, J.D. van Wyk, C.K. Campbell, and P.J. Wolmarans: "Power electronic interconnects: skin- and proximity effect-based frequency selective multipath propagation", *IEEE Trans. Power Electron*., Vol.20, No.3, pp.600–610 (2005)

(9) E. Finnansyah, S. Tomioka, S. Abel, M. Shoyama, and T. Ninomiya: "A critical-conduction-mode bridgeless interleaved boost power factor correction", Proc. IEEE Intl. Telecommunications Energy Conf. (INTELEC), pp.1–5 (2009)

(10) J.C. Hernandez, L.P. Petersen, and M.A.E. Andersen: "Characterization and evaluation of 600 v range devices for active power factor correction in boundary and continuous conduction modes", Proc. Appl. Power Electron. Conf. Expo. (APEC), pp.1911–1916 (2016)

(11) J.-W. Kim and G.-W. Moon: "Minimizing effect of input filter capacitor in a digital boundary conduction mode power factor corrector based on time-domain analysis", *IEEE Trans. Power Electron*., Vol.31, No.6, pp.3827–3836 (2016)

(12) Z. Liu, Z. Huang, F.C. Lee, and Q. Li: "Digital-based interleaving control for GaN-based MHz CRM totem-pole PFC", Proc. Appl. Power Electron. Conf. Expo. (APEC), pp.1847–1852 (2016)

(13) G. Ivensky, S. Bronshtein, and A. Abramovitz: "Approximate analysis of resonant LLC DC-DC converter", *IEEE Trans. Power Electron*., Vol.26, No.11, pp.3274–3284 (2011)

(14) G. Yang, P. Dubus, and D. Sadarnac: "Double-phase high-efficiency, wide load range high-voltage/low-voltage LLC DC/DC converter for electric/hybrid vehicles", *IEEE Trans. Power Electron*., Vol.30, No.4, pp.1876–1886 (2015)

(15) H. Li and Z. Jiang: "On automatic resonant frequency tracking in LLC series resonant converter based on zero-current duration time of secondary diode", *IEEE Trans. Power Electron*., Vol.31, No.7, pp.4956–4962 (2016)

(16) W. Zhang, F. Wang, D.J. Costinett, L.M. Tolbert, and B.J. Blalock: "Investigation of gallium nitride devices in high frequency LLC resonant converter", *IEEE Trans. Power Electron*., Vol.32, No.99 , pp.571–583 (2017)

(17) Y. Suzuki, I. Hasegawa, S. Sakabe, and T. Yamada: "Effective electromagnetic field analysis using finite element method for high frequency transformers with Litz-wire", Proc. IEEE Intl. Conf. Elect. Mach. Syst. (ICEMS), pp.4388–4393 (2008)

(18) V. Nabaei, S.A. Mousavi, K. Miralikhani, and H. Mohseni: "Balancing current distribution in parallel windings of furnace transformers using the genetic algorithm", *IEEE Trans. Magn*., Vol.46, No.2, pp.626–629 (2010)

(19) R. Krishnan, Switched reluctance motor drives, Boca Raton, FL, USA: CRC Press, pp.3–7 (2000)

(20) T.J.E. Miller: Electronic control of switched reluctance machines, Oxford, U.K.: Newns, pp.43–45 (2001)

(21) J.P. Vandelac and P.D. Ziogas: "A novel approach for minimizing high-frequency transformer copper loss", *IEEE Trans. Power Electron*., Vol.3, No.3, pp.266–277 (1988)

(22) J.A. Ferreira: "Appropriate modelling of conductive losses in the design of magnetic components", Proc. IEEE Power Electron. Specialist Conf. (PESC1990), pp.780–785 (1990)

(23) F. Robert and P. Mathys: "Ohmic losses calculation in SMPS transformers: numerical study of Dowell's approach accuracy", *IEEE Trans. Magn*., Vol.34, No.4, pp.1255–1257 (1998)

(24) W.G. Hurley, E. Gath, and J.G. Breslin: "Optimizing the AC resistance of multilayer transformer windings with arbitrary current waveforms", *IEEE Power Electron*., Vol.15, No.2, pp.369–376 (2000)

(25) J.T. Strydom and J.D. van Wyk: "Improved loss determination for planar integrated power passive modules", Proc. IEEE Appl. Power Electron. Conf. Expo. (APEC2002), Vol.1, pp.332–338 (2002)

(26) R. Pittini, Z. Zhang, and M.A.E. Andersen: "High current planar transformer for very high efficiency isolated boost DC-DC converters", Proc. IEEE Intl. Power Elecron. Conf. (IPEC2014), pp.3905–3912 (2014)

(27) M.A. Bahmani, T. Thiringer, and H. Ortega: "An accurate pseudoempirical model of winding loss calculation in HF foil and round conductors in switch-mode magnetics", *IEEE Trans. Power Electron*., Vol.29, No.8, pp.4231–4246 (2014)

(28) J.M. Lopera, M.J. Prieto, J. Diaz, and J. Garcia: "A mathematical expression to determine copper losses in switch-mode power supplies transformers including geometry and frequency effects", *IEEE Trans. Power Electron*., Vol.30, No.4, pp.2219–2231 (2015)

(29) T. Shirakawa, G. Yamasaki, K. Umetani, and E. Hiraki: "Copper loss analysis based on extremum co-energy principle for high frequency forward transformers with parallel-connected windings", Proc. Annu. Conf. IEEE Ind. Electron. Soc. (IECON2016), pp.1099–1105 (2016)

Tomohide Shirakawa (Student Member) was born in Nagasaki, Japan. He received the B. degree in electrical engineering from Okayama University, Okayama, Japan in 2015. His research interest includes magnetic analysis for magnetic components of high-frequency converters.

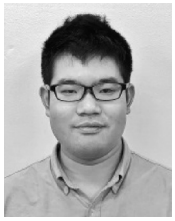

Genki Yamasaki (Student Member) was born in Okayama, Japan. He received the B. degree in electrical engineering from Okayama University, Okayama, Japan in 2016. His research interest includes operation analysis of DC-DC converters.

Kazuhiro Umetani (Member) was born in Kobe, Japan. He received the M. and Ph.D. degree in geophysical fluid dynamics from Kyoto University, Kyoto, Japan in 2004 and 2007, respectively. In 2015, he received the second Ph.D. degree in electrical engineering from Shimane University, Japan. From 2007 to 2008, he was a Circuit Design Engineer for Toshiba Corporation, Japan. From 2008 to 2014, he was with the Power Electronics Group in DENSO CORPORATION, Japan. He is currently an Assistant Professor at Okayama University, Okayama, Japan. His research interests include new circuit configurations in power electronics and power magnetics for vehicular applications. Dr. Umetani is a member of the Institute of Electrical and Electronics Engineers and the Japan Institute of Power Electronics.

Eiji Hiraki (Member) received the M.Sc. and Ph.D. degrees from Osaka University, Osaka, Japan, in 1990 and 2004, respectively. He joined Mazda Motor Corporation in 1990. From 1995 to 2013, he was with the Power Electronics Laboratory, Yamaguchi University, Yamaguchi, Japan. He is currently a Professor with the Electric Power Conversion System Engineering Laboratory, Okayama University, Okayama, Japan. His research interests include circuits and control systems of power electronics, particularly soft-switching technique for high-frequency switching power conversion systems. Dr. Hiraki is a member of the Institute of Electrical Engineers of Japan and the Japan Institute of Power Electronics.